SYNERGISTIC EFFECT ON COMBUSTION KINETICS AND ASH FUSION CHARACTERISTICS DURING CO-COMBUSTION OF BITUMINOUS COAL AND WHEAT STRAW

Miaomiao Niu[1,2*], Fengxia An[2], Ruize Shi[3], Xiangyu Xu[4], Yu Peng[1], Jingze Dong[1], Yuheng Liu[1]

[*1] College of Energy and Power Engineering, Nanjing Institute of Technology, Nanjing, 211167, China

[2] China Energy Science and Technology Research Institute Co., Ltd., Nanjing, 210023, China

[3] Jinan Heyuan Engineering Consulting Co., Ltd., Jinan, 250000, China

[4] Jiangsu Guoxin Shazhou Power Generation Co., Ltd., Suzhou, 215600, China

[*] Corresponding author; E-mail address: niumiao8899@163.com

In this study, the combustion behavior, synergistic effect and ash characteristics during the co-combustion of bituminous coal and wheat straw were fully analyzed by thermogravimetric analyzer, ash melting point analyzer, X-ray diffraction and scanning electron microscope. Thermogravimetry analysis showed that wheat straw was easier to be ignited, showing higher devolatilization activity and lower thermopositive temperature. Co-combustion displayed volatiles and char combustion stage and showed lower combustion rate compared to mono-combustion. For the wheat straw blending ratio≤50%, significant positive synergistic effect was observed during the volatiles combustion stage while negative synergistic effect was found during the char combustion stage. With wheat straw blending, the co-combustion ash fusion temperature first increased and then decreased. The mineral components of co-combustion ash gradually changed from high ash melting point compounds to complex calcium silicate hydrate. The morphology of co-combustion ash turned from hard flake structure to loose porous structure, showing partial melting in the biomass derived pores. Small addition of wheat straw during co-combustion would be beneficial to enhance the ash fusion temperature and optimize combustion performance.

Key words: *co-combustion; thermogravimetric analysis; synergistic effect; ash fusion; surface morphology; mineral transformation*

1. Introduction

Currently, coal is still the main source of energy and continues to dominate in the modern electricity generation. Increasing demands for carbon reduction and concerns over environmental problems have led to a shift from less environmental friendly fossil fuels to

renewable and sustainable energy alternatives[1]. Biomass is considered as the main clean and green energy which can reduce CO_2 emission and SO_2 atmospheric pollution due to its neutral carbon characteristic and less sulfur content, showing the advantages of wide distribution, low cost and renewability[2]. Co-combustion of biomass with coal is one of the most promising ways to utilize biomass in the existing coal-fired power plants with few modifications, which would be beneficial for combustion regulation, fuel cost saving and emission reduction.

Due to the large difference in chemical composition and calorific value, the combustion behavior of biomass and coal is quite different, making co-combustion challenging and unpredictable. Mureddu et al.[3] compared the detailed kinetics of various biomass and coal and found that biomass would change the ignition and burnout performance, thermal reactivity and kinetic behaviors of coal. Moon et al.[4] investigated the effect of biomass on co-combustion performance and found that 10% biomass addition enhanced the ignition of low-rank coal and promoted reactivity in the volatiles reaction. Jayaraman et al.[5] conducted thermogravimetric analysis of coal and biomass blends and detected the activation energy increased with biomass addition. However, considering the variable composition and low energy density of biomass, comprehensive analysis of combustion behavior and kinetics for typical biomass and coal were still insufficient for commercial application.

Furthermore, biomass was found to be easily slagging and fouling during mono-combustion due to the rich alkali and alkaline-earth metals (AAEMs) content. Co-combustion of biomass and coal may break the limit in biomass combustion temperature and overcome the serious ash-related problems of biomass combustion. Oladejo et al.[6] monitored the morphological change of coal-biomass ash fusion and revealed that high proportion coal blending could effectively mitigate the slagging propensity of individual biomass. Zhang et al.[7] found the ash fusion temperature first decreased and then increased with the addition of cow dung ash in coal ash, reaching a minimum value with 60% biomass ash addition. Unchaisri et al.[8] carried out circulating fluidized bed co-combustion of coal with various kinds of biomass and found that 50:50 rice straw/coal gave the highest deposit. So far, the mineral evolution and ash fusion characteristics during co-combustion are urgently needed to avoid slagging or deposition and optimize biomass/coal conversion efficiency.

Wheat straw is abundant and widely distributed in China. But the direct combustion of wheat straw currently faced several challenges, including low fuel energy density, unstable combustion, short equipment life (due to ash accumulation and slagging) and environmental pollution[9]. Co-combustion of wheat straw and coal may compensate for the deficiencies of individual combustion and integrate both fuel's advantages, resulting in clean, efficient and stable combustion[10, 11]. However, fundamental aspects such as combustion kinetics and synergistic interactions in wheat straw and coal co-combustion remain largely unexplored. In this paper, co-combustion of bituminous coal and wheat straw were fully analyzed in the view of combustion kinetics and ash characteristics. Non-isothermal thermogravimetry was used to clarify the co-combustion behavior and synergistic effect. The fusion temperature, composition and micro morphology of co-combustion ash were analyzed to get a full understanding of the melting characteristics, mineral composition and transformation.

2. Materials and methods

2.1. Raw materials

In this study, wheat straw (WS) from Shandong province and bituminous coal (BC) from Shaanxi province in China were selected as raw materials. Both samples were crushed to particle size no more than 0.3 mm and dried at 105℃ for 12 h to eliminate the disturbance of moisture. The proximate analysis of WS and BC sample was performed according to the Chinese standard GB/T 28731-2012 and GB/T 212-2008 respectively. The ultimate analysis of both samples was carried out by elemental analyzer (Thermo FLASH 2000). Both fuel properties are presented in Table 1.

Table 1 Properties of biomass and coal

Parameter	Proximate analysis (wt% air dry basis)				Ultimate analysis (wt% air dry basis)				
	Moisture	Volatile matter	Fixed carbon	Ash	C	H	O	N	S
WS	6.71	69.06	18.59	5.64	41.94	5.76	39.18	0.62	0.15
BC	6.46	31.86	56.11	5.57	71.21	6.29	8.96	0.87	0.65

2.2. Thermogravimetric analysis

Thermogravimetric analysis were conducted in a SDT650 thermogravimetric analyzer (TGA). For each test, the sample mass was kept at 6 ± 0.01 mg with a total air flow rate of 100 mL/min. The TGA temperature was increased from ambient temperature to 800°C at a heating rate of 20°C/min. The corresponding thermogravimetric (TG), differential thermogravimetric (DTG) and differential scanning calorimetry (DSC) curves of each sample were obtained. The combustion conversion of sample (on ash-free basis) at time t was expressed as α with a unit of % and calculated as follows:

$$\alpha=\frac{(w_0-w_t)}{(w_0-w_\infty)}\times 100\% \quad (1)$$

where w_0, w_t and w_∞ represent the initial, t time and final mass of the sample respectively, g. Flammability index (F), devolatilization index (D_i) and comprehensive evaluation index (S) were applied to reflect the ignition, devolatilization and comprehensive combustion characteristics. Higher value of F, D_i and S indicated better flammability, devolatilization and combustion performance, and vice versa. The parameters were calculated as follows.

$$F=\frac{(dw/dt)_{max}}{T_i T_p} \quad (2)$$

$$D_i=\frac{(dw/dt)_{max}}{T_i T_p \Delta T_{1/2}} \quad (3)$$

$$S=\frac{(dw/dt)_{max}(dw/dt)_{mean}}{T_i^2\times T_j} \quad (4)$$

where $(dw/dt)_{max}$ is the maximum combustion rate in %/min; T_i is the ignition temperature, ℃; T_p is the peak temperature for the maximum combustion rate, ℃; $\triangle T_{1/2}$ is the temperature interval when $dw/dt=1/2(dw/dt)_{max}$, ℃; T_j is the burnout temperature, ℃. $(dw/dt)_{mean}$ is the average combustion rate of the sample from T_i to T_j in %/min and could be calculated by:

$$(dw/dt)_{mean}=\beta\times\frac{(\alpha_j-\alpha_i)}{(T_j-T_i)} \quad (5)$$

where β is the heating rate of thermal experiment, °C/min; α_i and α_j are the values of initial conversion and termination conversion of combustion, respectively.

Combustion is a complex process due to the addition of oxygen, including volatiles reactions (devolatilization and combustion etc.) at low temperatures and char combustion at high temperature. In this context, a segmented kinetics scheme consisting of the two independent reaction stage is proposed for combustion. Kinetic parameters in each stage could be calculated for accurate assessment of the reaction activity. The reactions were governed by the first-order Arrhenius law, which has been used by other researchers for combustion kinetic analysis[12, 13]. The kinetics could be described as:

$$d\alpha/dt = kf(\alpha) \tag{6}$$

where k is the rate constant in the Arrhenius equation; $f(\alpha)$ is the model of reaction mechanism. A simple solid reaction mechanism function $f(\alpha) = (1-\alpha)^n$ was used for kinetic analysis, here n is the reaction order. The rate constant k could be calculated as follows:

$$k = A\exp(-E/RT) \tag{7}$$

where A is the pre-exponential factor, min^{-1}; E is the activation energy, kJ/mol; R is the gas constant, 8.314 J/(mol·K); T is the absolute temperature, K. During the combustion, a constant heating rate $\beta = dT/dt$ was used. Substitute β into the above equation and the kinetics would become:

$$d\alpha/dT = A/\beta \exp(-E/RT)\,(1-\alpha)^n \tag{8}$$

According to the Coats-Redfern integral method, for n=1, the kinetic equation can be integrated as:

$$\ln\left[\frac{-\ln(1-\alpha)}{T^2}\right] = \ln[AR/\beta E(1-2RT/E)] - E/RT \tag{9}$$

Since the $2RT/E$ was much less than 1, the expression $\ln[AR/\beta E(1-2RT/E)]$ was essentially constant. Thus $\ln\left[\frac{-\ln(1-\alpha)}{T^2}\right]$ has a linear relationship with $1/T$. Through the linear fitting of experimental data, the activation energy E and pre-exponential A can be calculated from the slope and intercept of the fitting line, respectively.

2.3. Ash preparation and analysis

The preparation of BC ash and WS ash was based on the Chinese standard GB/T 28731-2012 and GB/T 212-2008 respectively. For BC ash, BC was first heated up to 500°C within 50 min and held for 30 min. Then the temperature was further raised to 815°C and maintained for 2 h. For WS ash, WS was first heated to 250 °C at 5°C/min and maintained for 60 min. Then the sample was further heated to 550°C with at 5°C/min and kept for 3 h. The residence time at the final ashing temperature was extended by 1 h for both fuels to get adequate oxidation. Considering that carbon residue in the ash might affect the accuracy of ash fusion temperature measurements, for the blends ash, BC and WS was first thoroughly mixed and then ashed in the same way as BC. A high ashing temperature of 815°C can ensure the complete ashing of coal and release all the carbon from the blends.

Ash fusion temperature (AFT) tests were carried out using a TJHR-6000 ash fusion determinator (Tianjian, China) by carbon sealing method according to the Chinese standard GB/T 219-2008. The ash was shaped into triangular cone and heated from room temperature to 1500 °C for monitoring the ash cone shape changes. Four characteristic temperatures, including deformation temperature (DT), softening temperature (ST), hemispheric temperature (HT) and flow temperature (FT), were determined according to the real time images.

The mineral compositions of each ash were analyzed by an X-ray diffractometer (Rigaku SmartLab SE). The operation conditions of XRD were 40 kV and 40 mA Cu Kα radiation and step-scanned in the 2θ range of 10-80° with a speed of 10°/min. A Scanning Electron Microscope (Hitachi Regulus 8100) was used to obtain high-resolution secondary electron images and investigate the ash surface morphologies.

2.4. Synergistic effects calculation

Co-combustion interaction could be evaluated by calculating the difference between the experimental results and the theoretic results without synergy. Theoretical results are calculated according to the proportionally weighted average of the results measured from mono-combustion.

$$Y_{cal}=x_{BC}\times Y_{BC}+(1-x_{BC})\times Y_{WS} \quad (10)$$

Here, Y_{cal} is the weight-averaging calculated value; x_{BC} is the BC mass fraction in the feedstock blend; Y_{BC} is the experimental value of BC individual; Y_{WS} is the experimental value of WS individual.

To better evaluate the synergistic effect, the mean error (ME) was introduced as follows.

$$ME=\frac{\sum_{d=1}^{z}(Y_{exp}^{d}-Y_{cal}^{d})}{zY_{cal}^{mean}} \quad (11)$$

where Y_{exp}^{d} represents the experimental result measured by TG analysis at a time; Y_{cal}^{d} represents the calculated weight-averaging value based on the mono-combustion results at the time; d represents the serial number of the experimental data; z is the total number of the experimental data; Y_{cal}^{mean} represents the mean value of the calculated value.

3. Results and discussion

3.1. Co-combustion behavior analysis

3.1.1 Co-combustion characteristics

Figure 1 shows the thermogravimetric analysis of BC/WS co-combustion. Detailed combustion indexes are listed in Table 2. BC100/WS0, BC75/WS25, BC50/WS50, BC25/WS75 and BC0/WS100 represented the co-combustion with WS blending ratio of 0, 25%, 50%, 75% and 100% respectively. WS and BC were dried below 100°C and showed a small weight loss due to the water evaporation. WS was found to be ignited from 213°C and two distinguished weight loss stage were found. The first significant weight loss ranged from 213°C to 374°C, which was related to the high content of volatiles, hydrogen and oxygen of WS. Previous research has proved that the cellulose and hemicellulose in biomass started

decomposition above 160°C and turned into intense bond-breaking within 300-350°C[14]. The first WS combustion weight loss was mainly due to the volatiles releasing and combustion. Another WS weight loss occurred at 420-480°C, when the volatile matter was burnout but the remained char combustion started. During WS combustion, the thermopositive peak for volatiles combustion stage was wide and lower while the thermopositive peak for char combustion stage was short and high. Heat release of volatiles combustion was larger than that of char combustion. Different from WS, BC showed little weight change until about 300°C and started ignition from 458°C to 625°C. Only one-step weight loss occurred at the main BC combustion stage because of the high content of fixed carbon and low content of volatiles. DSC curves showed that the heat release of BC combustion was much larger than WS.

Comparing BC and WS, the maximum combustion rate of WS was higher than that of BC, which was in accordance with the combustion index results. Table 2 shows that the three combustion indexes of WS were all 5-8 times over those of BC, indicating a better ignition and combustion characteristics for WS combustion. The thermopositive process of BC combustion started from a higher temperature than WS, with the thermopositive peak temperature of BC larger than both those of WS. This might influence the biomass ash fusion during co-combustion.

Table 2 Combustion indexes for BC, WS and their blends

Parameter	**BC100/WS0**	**BC75/WS25**	**BC50/WS50**	**BC25/WS75**	**BC0/WS100**
T_i (°C)	458	283	253	235	213
T_p (°C)	552	548	303	303	304
T_j (°C)	625	600	583	565	487
$(dw/dt)_{max}$ (%/min)	12.6	8.6	11.9	13.0	16.3
$(dw/dt)_{mean}$ (%/min)	9.7	5.4	5.3	5.5	6.5
F (10^{-5}%·min^{-1}·°C^{-2})	4.98	5.58	15.57	18.23	25.18
D_i (10^{-7}%·min^{-1}·°C^{-3})	3.75	2.37	16.18	20.62	29.40
S (10^{-7}%^{2}·min^{-2}·°C^{-3})	9.30	9.75	16.91	22.72	47.88

As to co-combustion, Figure 1 shows the number of weight loss peak changed from one in BC combustion to two in co-combustion. The first peak temperature was gradually decreased with WS blending. The maximum co-combustion rate was lower than that of mono-combustion due to the separation of volatiles and char combustion. Based on the DSC analysis, two thermopositive peaks similar to WS combustion was found for co-combustion. The second thermopositive peak temperature decreased with WS blending since the char combustion started earlier. There was an observable fluctuation between the two expected thermopositive peaks, which might be attributed to the overtime volatiles combustion and advanced char combustion. The continuous heat release during co-combustion at high temperature was different from mono-combustion and may cause unexpected effect on ash fusion.

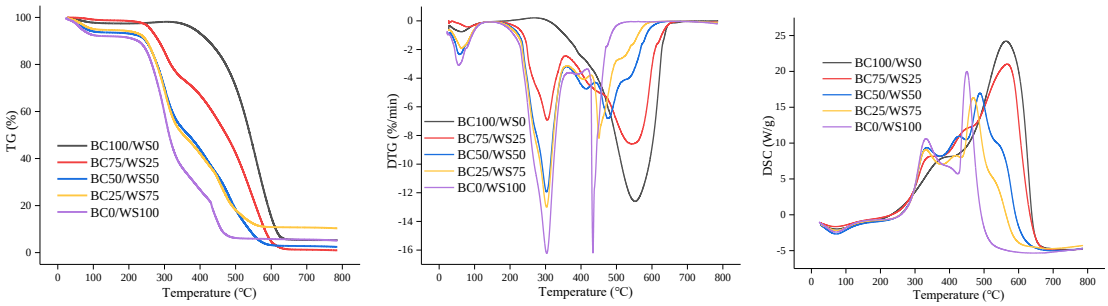

(a) TG curves (b) DTG curves (c) DSC curves

Figure 1 Thermogravimetric analysis of BC, WS and their blends

As shown in Table 2, the ignition temperature T_i for co-combustion was greatly decreased with WS blending. When the WS blending ratio was 25%, the improvement in flammability, devolatilization and combustion behavior was still limited. BC100/WS0 and BC75/WS25 basically showed similar combustion indexes. When the WS blending ratio kept increasing (50% and 75%), the combustion indexes and combustion rate were largely increased. Co-combustion with higher WS blending could reduce ignition difficulty and improve co-combustion reactivity due to the higher volatiles content in the blends. Overall, small addition of WS might modestly improve combustion while retain the BC combustion characteristics. With a higher blending ratio of WS, the devolatilization activity and combustion performance could be largely different from BC.

3.1.2 Kinetic analysis

Table 3 lists the kinetic parameters including the activation energy (E) and pre-exponential factor (A) for combustion tests. For all kinetic analysis, the regression coefficients (R^2) of fitting lines were in a range of 0.9798-0.9986, displaying good accuracy. BC combustion showed a single stage for both volatiles and char combustion at about 400-625℃. WS combustion and co-combustion all showed two separated stages for volatiles and char combustion respectively, which was mainly related to the high devolatilization reactivity of WS. Volatiles combustion occurred in 240-360℃ while char combustion mainly occurred in 430-500℃. BC75/WS25 combustion showed a particularly wide char combustion range from 465℃ to 590℃, proving that small addition of WS could extend the char combustion stage. BC50/WS50 combustion showed the minimum activation energy for both volatiles combustion and char combustion, reflecting a great interaction with equal fuel blending. At each stage, co-combustion basically displayed lower activation energy than BC combustion, especially for BC50/WS50 and BC25/WS75. With co-combustion, high reaction activity and flexible combustion range could be achieved.

Table 3 Kinetic parameters for combustion of BC, WS and their blends

Sample	Combustion stage	Range (℃)	E (kJ/mol)	A (min^{-1})	R^2
BC100/WS0	Volatiles and char	400-625	81.58	39580.48	0.9959
BC75/WS25	Volatiles	250-360	62.73	37135.65	0.9911
	Char	465-590	55.93	1116.22	0.9798
BC50/WS50	Volatiles	240-350	47.38	2565.90	0.9985

	Char	460-510	32.71	38.55	0.9973
BC25/WS75	Volatiles	240-350	52.66	10073.25	0.9982
	Char	435-480	38.03	141.43	0.9986
BC0/WS100	Volatiles	240-355	47.79	4279.61	0.9939
	Char	425-460	63.23	27003.48	0.9976

3.1.3 Synergistic effect

Figure 2 shows the synergy of BC and WS during co-combustion. Similar experimental and theoretical TG, DTG and DSC trends were observed but some difference in combustion rate and heat change were still existed, especially for the WS blending of 25% and 50%. BC75/WS25 showed higher co-combustion rate than the theoretical value in the whole range. The positive synergistic effect was remarkable for volatiles combustion, and gradually decreased with char combustion. With WS-volatiles evaporation at low temperature, the AAEMs of WS could be released and act as catalysts for promoting BC-volatiles decomposition. At higher temperature (approximately > 400℃), the volatiles release was basically complete and interaction between WS char and BC char was weakened[15].

For BC50/WS50, the co-combustion rate showed obvious positive synergistic effect during volatiles combustion. The maximum volatiles co-combustion rate was 1.5 times of the theoretical value, with the maximum rate temperature consistent with the theoretical value. Interaction was also observed in char combustion, displaying two weight loss peaks at 413℃ and 476℃ earlier than the theoretical value of 434℃ and 551℃. Kastanaki et al. compared the structure and kinetic characteristics of biomass char and coal char. They found that the biomass char were more active than coal and could be burned at lower temperature[16]. The skeleton structure of biomass char was more easier to be broken down and produced much more small gas molecules than coal at the same temperature, leading to cracking-burning-cracking chain reactions and accelerating char combustion. Thus the char combustion would occur earlier during co-combustion, meaning lower activation energy needed for char co-combustion. As shown in Table 3, the activation energy for char combustion stage during co-combustion was lower than that during individual combustion. The dramatic volatiles/char combustion stimulated heat release and the actual heat release of co-combustion was relatively high. For BC25/WS75, the co-combustion synergy between WS and BC was greatly diminished. The actual TG, DTG and DSC curves during volatiles release/combustion stage were almost identical to the theoretical curves until 400℃. There were still some interaction in the char combustion stage, showing a lower actual char combustion rate.

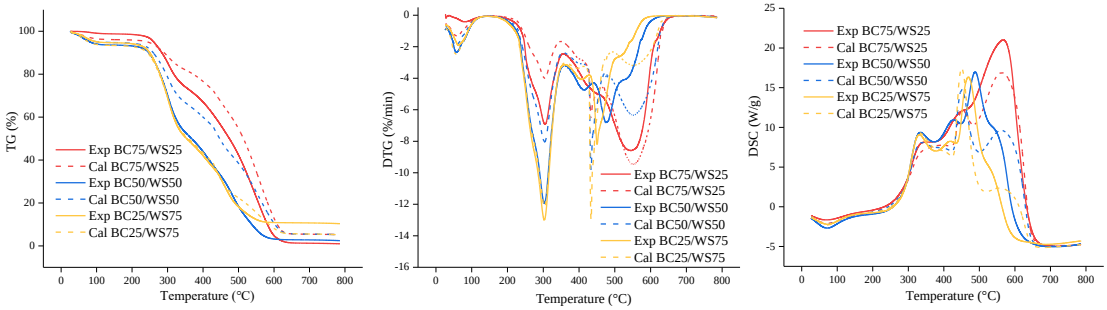

(a) TG synergy (b) DTG synergy (c) DSC synergy

Figure 2 Synergy between BC and WS during co-combustion

Complex combustion synergy between BC char and WS char was found for both three blends combustion due to large difference in char structure and composition. Theoretical linear fitting of the two fuels resulted in multiple weight loss peaks and different co-combustion rates in char combustion stage. However, there was only one obvious weight loss peak and several reaction weight loss steps in actual char combustion. For example, all three conditions showed a theoretical weight loss peak at about 550℃. But only BC75/WS25 showed a similar experimental weight loss peak. Although there were still some combustion rate fluctuations at 500-600℃, WS blending has greatly advanced the char combustion and weakened high temperature combustion. The interaction of WS and BC has formed a region for both char combustion.

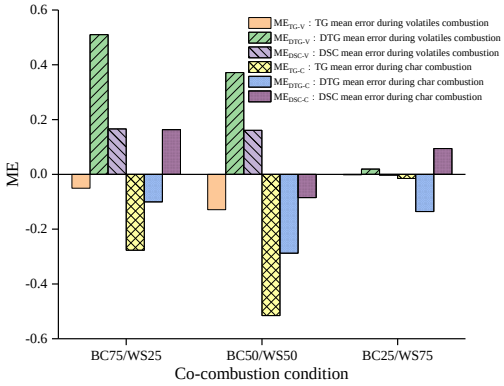

Figure 3 Co-combustion mean error for thermogravimetric analysis

Figure 3 shows the mean error for volatiles combustion and char combustion based on TG, DTG and DSC results. BC50/WS50 exhibited significant synergy for both stages. A positive MR was obtained for DTG results during volatiles combustion, indicating a positive synergy for volatiles co-combustion. Although advanced char combustion and lower activation energy was observed for BC50/WS50 combustion, the DTG and DSC results failed to reach the theoretical value, reflecting a negative synergy on char co-combustion. This might be related to the competitive mechanism between BC-char and WS-char during gas-solid reactions with oxygen or volatiles. Although the AAEMs in WS could weaken the polymer chain and catalyze WS-char combustion, the presence of BC-char hindered the diffusion of the WS-char flame, thereby exhibiting a flame retardant effect for co-combustion[17]. In addition, due to the influence of WS-char, BC-char started burning at a lower temperature, which limited the combustion reactivity and further reduced the co-combustion rate. Small addition of WS (25%) may promote the rapid decomposition of BC volatiles and accelerated volatiles combustion. With a higher WS blending ratio (75%), the volatiles combustion of WS has taken a dominated part and the devolatilization of BC showed little effect on co-combustion. For BC25/WS75, little synergy was found for volatiles combustion and negative synergy was observed for char combustion. Overall, the co-combustion of BC and WS resulted in different synergistic effect for the volatiles and char combustion.

3.2. Ash fusion characteristics

3.2.1 Ash fusion temperature

Ash fusion temperature could reflect the melting possibilities of different blending fuels and greatly affect the co-combustion performance. Table 4 shows the ash fusion temperature of the five kinds of ash. BC ash showed higher DT, ST, HT and FT than WS ash. WS ash started deformation at 1017℃, which was about 130℃ lower than BC ash. Thus, WS ash was more easily to be melted and agglomeration would first occur during WS combustion. In fact, biomass agglomeration during thermochemical conversion has been found in many research[18]. BC ash showed a narrow ash fusion range of 55℃ from deformation to flowing, while WS ash showed a wider range of 89℃. For BC/WS blends, the ash fusion temperature first showed a great increase with 25% WS blending, showing a deformation temperature even higher than that of BC ash. The flow temperature of BC75/WS25 ash was also much higher than that of mono-combustion ash, reaching a maximum temperature of 1264℃. Yang et al. studied the co-melting ash behavior of municipal solid waste (MSW) and coal and observed that with specific blending ratio the ash fusion temperature of the blended ash could be higher than that of both MSW ash and coal ash[19]. This might be related to the high-temperature eutectic zone formed during co-melting. When WS blending ratio ⩾50%, the ash fusion temperature turned to decline. BC50/WS50 ash displayed a flow temperature very close to BC ash while its deformation started much earlier. Each ash fusion temperature of BC25/WS75 ash tended to be 30-40℃ above that of WS ash. Furthermore, all three blend ashes showed wider ash fusion range than mono-combustion ash. The maximum ash melting range (113℃) was found in BC75/WS25 ash, which could be regarded as a combined effect of both BC and WS ash.

Table 4 Ash fusion temperature of different ash

Ash sample		DT(℃)	ST(℃)	HT(℃)	FT(℃)
BC100/WS0 ash	Experimental value	1145	1168	1176	1200
BC75/WS25 ash	Theoretical value	1113	1139	1150	1177
	Experimental value	1151(↑38)	1213(↑74)	1238(↑88)	1264(↑87)
BC50/WS50 ash	Theoretical value	1081	1110	1125	1153
	Experimental value	1095(↑14)	1127(↑17)	1142(↑17)	1195(↑42)
BC25/WS75 ash	Theoretical value	1049	1081	1099	1130
	Experimental value	1046(↓3)	1091(↑10)	1115(↑16)	1153(↑23)
BC0/WS100 ash	Experimental value	1017	1052	1073	1106

For each co-combustion ash, the experimental ash fusion temperature was higher than the theoretical value, especially for BC75/WS25 ash. This fully proved the interaction between the inorganic components of BC and WS during co-combustion. The increase of ash fusion temperature would be beneficial to avoid the risk of ash slagging and accumulation, showing positive effect for biomass utilization. With WS blending, the synergistic effect on ash fusion was gradually weakened and the difference between experimental and theoretical ash fusion temperature became smaller. For WS blending ratio⩾50%, the blends still showed higher ash fusion temperature than WS. But compared to BC ash, the initial deformation temperature of

blends ash was decreased, which extended the melting stage and may cause some slagging problems.

3.2.2 Mineral transformation behavior

The ash derived from BC, WS and their blends were characterized by XRD and shown in Figure 4. Significant mineral differences were observed among the five ash samples. The main mineral of BC ash were SiO_2, $CaSO_4$ and gismondine ($CaAl_2Si_2O_8!4H_2O$). The formation of gismondine may be related to the weak bond of SiO_2 and Al_2O_3 and the destroy of crystalline structure. These minerals would be melted together and transformed to gismondine[20]. The melting temperatures of SiO_2 and $CaSO_4$ were 1610℃ and 1000-1200℃ respectively[21]. As one kind of zeolite-type minerals, gismondine showed a melting temperature between 800-1200°C[22]. The coal ash showed a relatively high ash fusion temperature due to these high temperature melting minerals. For WS ash, there were K_2SO_4, $Al(OH)_3$, reyerite ($(Na,K)Ca_7Si_{11}AlO_{29}(OH)_4!H_2O$) and brownmillerite ($Ca_2(Al,Fe^{+3})_2O_5$) etc. Compared to BC ash, more kinds of minerals containing AAEMs were found in the WS ash, which would greatly decrease the melting temperature of WS ash[23]. Besides, the existence of K_2SO_4 could influence the melting temperature by forming low temperature eutectics with temperature[24]. All these have led to a lower ash fusion temperature for WS ash.

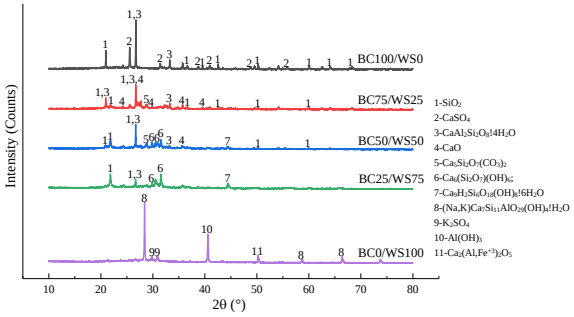

Figure 4 XRD patterns of ash from BC, WS and their blends

As shown in Figure 4, the main minerals (SiO_2 and gismondine) of BC ash were still detected while no mineral containing alkali metals were found in the blended ash, suggesting that alkali metals may have all been volatilized due to the high ashing temperature for co-combustion. Strong diffraction peak for CaO, SiO_2 and gismondine were detected in BC75/WS25 ash. CaO was mainly derived from the interaction between BC and WS minerals. With a melting temperature of 2570℃, the existence of CaO could largely enhance the ash fusion temperature of BC75/WS25 ash. In addition, compared with BC ash, the enrichment degree of SiO_2 and gismondine was increased for BC75/WS25 ash and further increased the ash fusion temperature. Therefore, the ash fusion temperature of BC75/WS25 ash was even higher than that of BC ash. With WS blending, the diffraction peaks for SiO_2 and gismondine were gradually decreased and CaO was not found for WS blending of 50% and 75%. New types of calcium silicate hydrates were detected for BC50/WS50 ash and BC25/WS75 ash, including jaffeite ($Ca_6(Si_2O_7)(OH)_6$) and jennite ($Ca_9H_2Si_6O_{18}(OH)_8!6H_2O$). This might be related to the change of Si/Ca ratio and AAEMs content in the blended ash, which may affect the mineral transformation and promote the formation of low temperature eutectics. For WS blending ratio

higher than 50%, the ash minerals turned from high melting temperature compounds to more complex eutectics.

3.2.3 *SEM analysis (Surface morphology)*

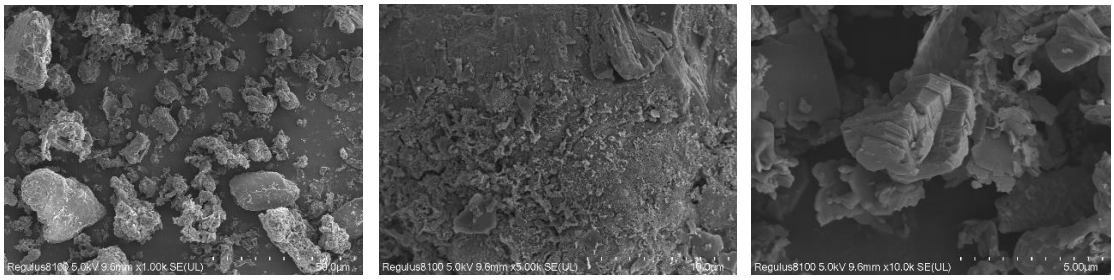

(a) BC100/WS0 ash (×1000) (b) BC100/WS0 ash (×5000) (c) BC100/WS0 ash (×10000)

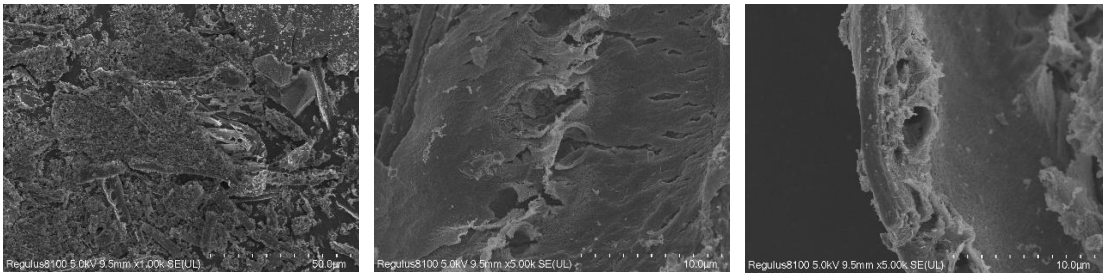

(d) BC0/WS100 ash (×1000) (e) BC0/WS100 ash (×5000) (f) BC0/WS100 ash (×5000)

Figure 5 Typical surface morphologies of mono-combustion ash

Figure 5 shows the typical surface morphologies of BC ash and WS ash with different magnifications. BC ash were distinct and dense particles with the surface texture varying from coarse to smooth. No significant sintering or melting aggregation were observed in BC ash. WS ash were more loose, porous and rough particles with lamellar morphology and brittle texture. The rough surface of WS ash might be related to the sintering of biomass at high temperature, as shown in Figure 5(d). The porosity of WS ash was mainly due to the high volatiles content of WS and intense devolatilization. Minor melt phase were detected inside the pore, suggesting that partial melting could occur at temperature much lower than the deformation temperature. Significant melting usually appeared with large pores. The decomposition and combustion could release large amount of heat in a small space and stimulate the fusion of nearby ash.

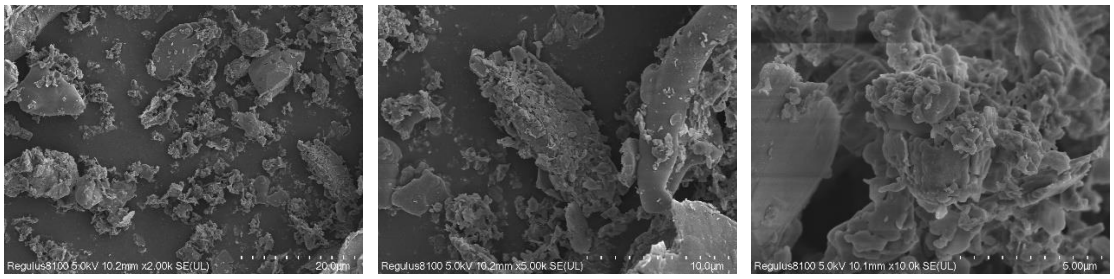

(a) BC75/WS25 ash (×2000) (b) BC75/WS25 ash (×5000) (c) BC75/WS25 ash (×10000)

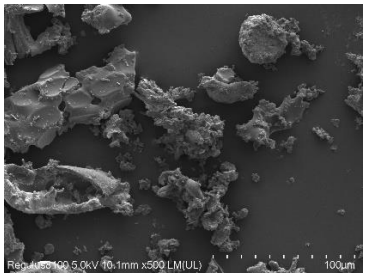
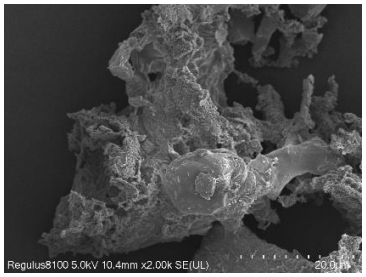
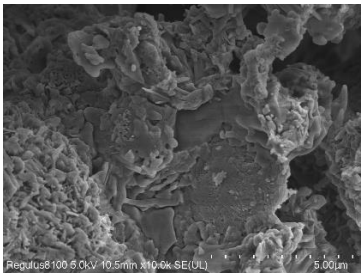

(d) BC50/WS50 ash (×500) (e) BC50/WS50 ash (×2000) (f) BC50/WS50 ash (×10000)

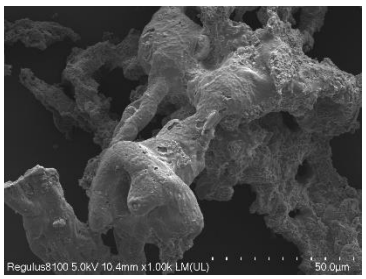

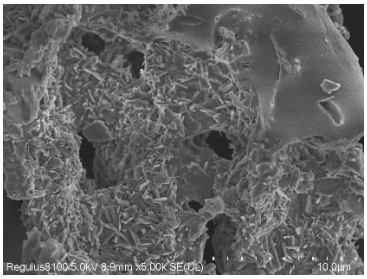

(g) BC25/WS75 ash (×1000) (h) BC25/WS75 ash (×5000) (i) BC25/WS75 ash (×10000)

Figure 6 Typical surface morphologies of co-combustion ash

The typical surface morphologies of co-combustion ashes are shown in Figure 6. Since the co-combustion ashes were all prepared according to the coal ashing method (heating to 815℃), partial melting was observed for all three ashes. As to BC75/WS25 ash, a large proportion of particles showed similar shape as BC ash while a few particles showed increment in surface weathering, roughness, micro-cracks and porosity. Melting mostly occurred in the WS derived ash due to intense devolatilization. As to BC50/WS50 ash, some particles displayed large and regular shape with smooth surface. The others were formed by agglomeration of loose and fibrous surface grains. The distinction between BC derived ash and WS derived ash was blurring and most ash particles showed an aggregation state. For WS blending ratio of 75%, the ash was obviously molten and displayed relatively smooth surface. The concentrated heat release of WS and high amount of alkali metals resulted in large number of pores with different sizes and ash melting in the pore.

4 Conclusion

In this paper, thermogravimetric analysis, ash fusion characteristics, X-ray diffraction and SEM analysis were carried out to understand the co-combustion behavior and ash evolution during co-combustion of BC and WS with different WS blending. The introduction of WS successfully reduced ignition difficulty by increasing volatile matter content. The devolatilization activity of co-combustion was greatly improved compared to BC combustion. Positive synergistic effect on volatiles combustion and heat release were found during co-combustion, especially for WS blending ratio≤50%, while negative synergistic effect on char combustion and heat release were found. Co-combustion with small addition of WS could effectively avoid the agglomeration problems due to its higher ash fusion temperature. The

alkali metals in WS ash was volatilized and ash minerals turned from high ash melting temperature compounds to more complex eutectics. Partial melting was increased with WS blending and the ash morphology was determined by the fuel with high blending ratio.

Acknowledgement

The authors acknowledge the financial support from the National Natural Science Foundation of China (51906100, 12305186), the Natural Science Foundation of Jiangsu Province (BK20191015), the Innovation Foundation of Nanjing Institute of Technology (CKJA202302) and the Open Foundation of State Key Laboratory of Low-carbon Smart Coal-fired Power Generation.

Reference

[1] Deonarine, A., et al., Environmental Impacts of Coal Combustion Residuals: Current Understanding and Future Perspectives. Environmental Science & Technology, 2023. 57(5): pp. 1855-1869.
[2] Antar, M., et al., Biomass for a sustainable bioeconomy: An overview of world biomass production and utilization. Renewable and Sustainable Energy Reviews, 2021. 139: pp. 110691.
[3] Mureddu, M., et al., Air-and oxygen-blown characterization of coal and biomass by thermogravimetric analysis. Fuel, 2018. 212: pp. 626-637.
[4] Moon, C., et al., Effect of blending ratio on combustion performance in blends of biomass and coals of different ranks. Experimental Thermal and Fluid Science, 2013. 47: pp. 232-240.
[5] Jayaraman, K., et al., Thermogravimetric and mass spectrometric (TG-MS) analysis and kinetics of coal-biomass blends. Renewable Energy, 2017. 101: pp. 293-300.
[6] Oladejo, J. M., et al., In-situ monitoring of the transformation of ash upon heating and the prediction of ash fusion behaviour of coal/biomass blends. Energy, 2020. 199: pp. 117330.
[7] Zhang, L., et al., Influence of biomass ash additive on fusion characteristics of high-silicon-aluminum coal ash. Fuel, 2020. 282: pp. 118876.
[8] Unchaisri, T. and Fukuda, S., Investigation of ash formation and deposit characteristics in CFB co-combustion of coal with various biomass fuels. Journal of the Energy Institute, 2022. 105: pp. 42-52.
[9] Taghizadeh-Alisaraei, A., et al., Potential of biofuels production from wheat straw biomass, current achievements and perspectives: a review. Biofuels, 2023. 14(1): pp. 79-92.
[10] Chaudhuri, P., et al., Unravelling bioenergy potential of bamboo and bamboo bio-char through thermogravimetric analysis. Energy Sources, Part A: Recovery, Utilization, and Environmental Effects, 2025. 47(1): pp. 10601-10612.
[11] Milićević, A., et al., Mathematical modelling and optimisation of lignite and wheat straw co-combustion in 350 MWe boiler furnace. Applied Energy, 2020. 260: pp. 114206.
[12] Wang, Q., et al., Reactivity and Kinetic Analysis of Biomass during Combustion. Energy Procedia, 2012. 17: pp. 869-875.
[13] Tong, W., et al., Experiment and expectation: Co-combustion behavior of anthracite and biomass char. Bioresource Technology, 2019. 280: pp. 412-420.
[14] Zhu, L. and Zhong, Z., Effects of cellulose, hemicellulose and lignin on biomass pyrolysis kinetics. Korean Journal of Chemical Engineering, 2020. 37(10): pp. 1660-1668.
[15] Caliskan Sarikaya, A., et al., Synergistic Interactions During Cocombustion of Lignite, Biomass, and Their Chars. Journal of Energy Resources Technology, 2019. 141(12): pp. 122203.
[16] Kastanaki, E. and Vamvuka, D., A comparative reactivity and kinetic study on the combustion of coal–biomass char blends. Fuel, 2006. 85(9): pp. 1186-1193.
[17] Cong, H., et al., Evaluating the performance of honeycomb briquettes produced from semi-coke and corn stover char: Co-combustion, emission characteristics, and a value-chain model for rural China. Journal of Cleaner Production, 2020. 244: pp. 118770.

[18] He, Z.-M., et al., Review of Biomass Agglomeration for Fluidized-Bed Gasification or Combustion Processes with a Focus on the Effect of Alkali Salts. Energy & Fuels, 2022. 36(16): pp. 8925-8947.
[19] Yang, G., et al., Co-melting properties and mineral transformation behavior of mixtures by MSWI fly ash and coal ash. Journal of the Energy Institute, 2021. 96: pp. 148-157.
[20] Che Pa, F. and Mohamad Nasir, N. N. *Synthesis of Zeolite from Rice Husk Ash*. in *Proceedings of the Green Materials and Electronic Packaging Interconnect Technology Symposium*. 2023. Singapore: Springer Nature Singapore.
[21] Deng, S., et al., Ash fusion characteristics and mineral matter transformations during sewage sludge/petrochemical sludge co-firing with wheat straw. Journal of Cleaner Production, 2020. 260: pp. 121103.
[22] Wang, T., et al., Regulation of ash slagging behavior for sewage sludge by rice husk addition: Focusing on control mechanisms. Journal of Cleaner Production, 2021. 284: pp. 124677.
[23] Lu, Y., et al., Investigation on the ash characteristics and AAEM migration during co-combustion of Zhundong coal and shale char in a fixed bed. Fuel, 2022. 327: pp. 125214.
[24] Xiao, H., et al., Effect of potassium-containing sulfates on high-temperature mineral transformation and coal ash fusibility. Energy Sources, Part A: Recovery, Utilization, Environmental Effects, 2024. 46(1): pp. 12496-12511.

Submitted: 14.03.2025.
Revised: 18.06.2025.
Accepted: 19.06.2025.